Energy 268 (2023) 126728

Contents lists available at ScienceDirect

Energy

journal homepage: www.elsevier.com/locate/energy

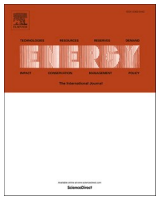

Investigation of control strategies for adsorption-based CO_2 capture from a thermal power plant under variable load operation

Vidar T. Skjervold [a,*], Giorgia Mondino [b], Luca Riboldi [c], Lars O. Nord [a]

[a] NTNU - Norwegian University of Science and Technology, Department of Energy and Process Engineering, Trondheim, Norway
[b] SINTEF Industry, P.O. Box 124, Blindern, N0314, Oslo, Norway
[c] SINTEF Energy Research, Sem Sælands vei 11, 7034, Trondheim, Norway

ARTICLE INFO

Handling Editor: Petar Sabev Varbanov

Keywords:
CO_2 capture
Temperature-swing adsorption
Moving bed
Variable load
Process control
Dynamic simulations

ABSTRACT

This work considers the closed-loop behavior of a moving bed temperature swing adsorption process designed to capture CO_2 from a coal-fired power plant. Four decentralized control strategies were studied based on step changes and ramps of flue gas feed flow rate and controller setpoint changes. A proportional-integral (PI) control configuration, where CO_2 purity was controlled by hot fluid velocity to the desorption section and CO_2 recovery was controlled by the sorbent flow rate, demonstrated the overall best performance. The 99% settling time for higher-level control variables varied from 0 to 13 min for most control configurations and the settling time for CO_2 purity was generally longer than for CO_2 recovery. The simulations show that using ratio controllers lead to larger offsets but can give around 10 times faster purity response compared to PI-control. All investigated control combinations were able to keep the controlled variables relatively close to the setpoints and the largest relative steady state setpoint offset was 2%.

1. Introduction

1.1. Background and motivation

To mitigate the effects of global warming, CO_2 emissions need to be significantly reduced over the coming decades. The transition to a low-carbon energy system will impact the operation of thermal power plants in several ways. Firstly, it is expected that variable renewable energy sources will stand for an increasing share of electricity production. Based on announced policies and targets, the International Energy Agency recently estimated that renewables will make up 80% of the growth in global electricity demand in the next decade [1]. Furthermore, they expect nearly 40% of the global electricity demand in 2030 to be covered by the combination of hydro, wind, solar, bioenergy, geothermal and marine power. The intermittency of such electricity sources represents a challenge for the electrical grid since supply and demand must balance. The residual load can be met by fossil power plants [2], which need to operate at varying loads due to the lack of large-scale energy storage solutions [3]. Ensuring reliability of supply will be important to achieve a fair energy transition, which is a key aspect of the United Nations Sustainable Development Goal 7 on affordable and clean energy [4].

It is likely that the deployment of CO_2 capture on thermal power plants will be necessary to meet our climate targets. As an example, a recent IPCC report shows a wide range of carbon capture and storage deployed on both natural gas and coal-fired power plants across pathways compatible with the 1.5 °C global warming scenario [5]. Post-combustion capture technologies are suitable for retrofit to existing plants, and the most mature technology is absorption-based CO_2 capture with chemical solvents [6]. However, due to the absence of large amounts of water, adsorption-based capture technologies could have lower regeneration duties [7], which would reduce the penalty on the power plant efficiency caused by integration with the CO_2 capture process.

This work considers post-combustion CO_2 capture by the moving bed temperature swing adsorption (MBTSA) technology. One of the main features distinguishing the moving bed configuration from the conventional fixed bed systems is that the former can be operated continuously. This is beneficial because it renders complex cycle schedules unnecessary and eliminates the parasitic energy losses associated with intermittent heating/cooling of the heat exchanger walls. The possibility to operate continuously is also an advantage in terms of internal heat recovery, process integration with the power plant, and process control. However, in the context of CO_2 capture from a load-following power

* Corresponding author.
E-mail address: vidar.t.skjervold@ntnu.no (V.T. Skjervold).

https://doi.org/10.1016/j.energy.2023.126728
Received 28 February 2022; Received in revised form 3 November 2022; Accepted 14 January 2023
Available online 17 January 2023

plant, the MBTSA process will frequently deviate from nominal operation due to disturbances from the power plant. In the work presented by Kim et al. a one-dimensional, non-isothermal model was used to study the response of the MBTSA process regeneration step to disturbances typical for power plants [8]. Since only a part of the process was studied, a complete picture of the dynamic behavior of the system is not obtained. The complete MBTSA process including adsorption, desorption and cooling is studied in a paper by Morales-Ospino et al. [9]. A parametric analysis was used to investigate the effect of several variables on the key performance parameters of the process. Using a similar modelling approach, the MBTSA process was studied in a coal-fired power plant context [10] and for a natural gas combined cycle power plant [11]. These studies do not consider the operation of the CO_2 capture system away from the steady state.

A control system is required to keep the operation of the MBTSA process stable during variations in power plant operation. As evidenced by the review of Wu et al. [12], both conventional, decentralized feedback controllers and advanced model predictive control approaches have been widely studied for post-combustion CO_2 capture. A summary of relevant literature is given in the following sections.

1.2. Decentralized control of post-combustion CO_2 capture

The control system is often divided into two main parts: a regulatory control layer aiming at stabilizing operation and a higher-level control layer aiming at maintaining performance. The regulatory layer includes sump levels, column pressures, reboiler, condenser and lean solvent temperatures, makeup water and solvent flows [12]. A decentralized control approach is based on single input – single output loops, where one manipulated variable (MV) is needed for each controlled variable (CV). The regulatory layer therefore leaves only a few degrees of freedom to be used as MVs in the higher-level control layer. The most common approach is to use the solvent circulation rate and flow rate of steam as MVs and CO_2 capture rate and a temperature somewhere in the process (e.g. the reboiler) as CVs for higher-level control [13].

Most of the studies in the literature focus on modelling and control of only the post-combustion capture process, meaning that variations in power plant operation are treated as external disturbances to the system. Cormos and her group carried out a comparison of proportional-integral (PI) control with model predictive control (MPC) based on step changes in inlet flue gas flow rate [14]. The solvent flow rate was used to control the sweet gas CO_2 concentration, which is closely linked to the CO_2 capture rate. No significant difference in performance between the feedback control and MPC scheme was observed. A similar conclusion was found by Panahi and Skogestad, who recommended a simple control structure over MPC due to similar performance and easier implementation [15]. Gaspar and coworkers presented a comparison of control of piperazine-based and monoethanolamine (MEA) based capture systems under varying power plant load, valve disturbance in the lean solvent stream and reduced heat delivery [16]. The CO_2 capture rate was controlled by manipulating the solvent flow rate. Similar control pairings are used in other research studies that analyzed MEA-based capture processes under various disturbances [17–19]. In these studies, the reboiler temperature is also included in the control scheme, paired with the reboiler duty. Lawal et al. considered switching off water balance control, increased flue gas flow, reduced reboiler duty and increased flue gas CO_2 concentration [17]. Lin et al. studied changes in water makeup flow, flue gas flow rate and CO_2 capture rate setpoint [18]. Mechleri and coworkers considered positive and negative changes in flue gas flow rate [19]. In the work presented by Nittaya et al. the reverse pairing is also considered, i.e. using reboiler duty to control CO_2 capture rate and solvent flow (both lean and rich) to control reboiler temperature [20]. A heuristic pairing philosophy was found to give the best controller performance. Cristea et al. presented an augmented CO_2 capture process with an additional solvent buffer tank and auxiliary heat exchanger to reduce interactions within the system [21]. A decentralized control system was investigated and shown to be reliable for disturbances in flue gas flow rate and inlet CO_2 concentration as well as CV setpoint changes.

In a few articles, coupled models of the power plant and post-combustion CO_2 capture system are used to study the integrated system under dynamic conditions [13,22–24]. In addition to the flue gas flowing from the power plant to the capture process, these models consider the extraction of steam from the power plant (typically in the cross-over between the intermediate and low-pressure turbines) and the return of condensate to the boiler feedwater line. Mechleri et al. investigated coupled models of both a supercritical, pulverized coal power plant and a natural gas combined cycle power plant with the capture process [22]. In addition, the CO_2 compression is included in the model. Feedback control strategies similar to the ones reported by Nittaya et al. (i.e., capture rate controlled by the reboiler duty and reboiler temperature by solvent flow) [20] are employed, in addition to a case with dynamic switching between modes. A supercritical coal-fired power plant with MEA-based capture is also considered by Gardarsdottir et al. [13]. In addition to the standard MV-CV pairings, the authors include a control strategy that replaces the CO_2 capture rate with the liquid to gas ratio as control objective and a case where the solvent flow is kept constant. These control alternatives are also studied for a natural gas combined cycle (NGCC)-MEA system, in addition to feedforward (ratio) controllers for the solvent and reboiler steam flow [23]. A subcritical coal-fired power plant coupled to an amine solvent CO_2 capture process is studied by Lawal et al. [24], using the same control system as in their previous work, i.e., by manipulating the solvent flow rate [17].

1.3. Model predictive control of post-combustion CO_2 capture

In model predictive control, a centralized approach is applied at every time step to determine the optimal control action for a given predictive horizon [12]. As the name suggests, MPC requires a predictive dynamic model of the post-combustion CO_2 capture system, providing the future values of CVs based on the current state and future values of the MVs. If a linear predictive model is used, the control method is referred to as linear model predictive control (LMPC). Similarly, in non-linear model predictive control (NMPC) a non-linear process model is applied. The best control inputs at a given time step are determined by solving a dynamic optimization problem consisting of an objective function and constraints on the input and output variables. The objective function usually reflects the control performance [25], containing terms penalizing deviations from the controller setpoints and large changes in the manipulated variables (aggressive controller action) [26]. Several recent studies have considered MPC for post-combustion CO_2 capture.

In the case of LMPC, a quadratic programming optimization solver can often be used to determine the control action, since the predictive model is linear and the objective function is often quadratic. This reduces the computational demand of the controller [27] compared to NMPC. Li and coworkers found LMPC to give better setpoint tracking and less aggressive input usage compared to traditional PID control for an MEA-based capture process with the CO_2 capture rate as the only control objective [28]. Based on a first-principle model validated with pilot-scale experimental data, Jung et al. applied gap metric analysis and developed a linear predictive model around the optimal reference point for linearization [27]. Three LMPC controller options were studied for set point changes and flue gas flow disturbances. The same group used a state-space predictive model to study LMPC for an amine-based capture process with an advanced flash stripper [29]. The model predictive controller was found to outperform decentralized control structures. LMPC for an entire NGCC plant with integrated post-combustion capture was studied by Rua et al. [26]. The predictive model consisted of several linear autoregressive with exogeneous input (ARX) models that were combined in a local model network using a Gaussian validity function to weigh the individual contributions. The MPC was found to outperform the PID control approach from a previous study [23]. Sultan and coworkers increased the computational efficiency of an LMPC by solving

the quadratic programming problem in smaller fragments [30]. They compared the "fast model predictive controller" to a conventional approach and reported shorter settling times and smaller setpoint deviations.

In cases where the controller should be applicable to a wide range of operation, NMPC might be necessary in order to capture the non-linear dynamics of the post-combustion CO_2 capture process [12]. Wu et al. developed a first-principle model of a solvent-based capture process in gPROMS and identified a non-linear artificial neural network prediction model via a feed-forward back propagation method [25]. Particle swarm optimization was applied to determine controller settings. The NMPC was tested for disturbances in flue gas flow rate and compared to LMPC based on a state-space model. In another study, a nonlinear autoregressive with exogeneous input (NARX) model was used for prediction [31]. NMPC was compared to LMPC for variations in flue gas flow rate and CV setpoints and found to give better performance. Patron and Ricardez-Sandoval considered the absorber unit of a post-combustion CO_2 capture system and applied a multi-scenario NMPC where uncertainties were taken into account in the optimization step of the control algorithm [32]. Mejdell and coworkers tested the commercial NMPC software CENIT at the Tiller pilot plant in Norway, concluding that the control system was able to handle both setpoint changes and disturbance rejection [33].

The optimization problem used to determine controller action can contain terms related to the economics of the process, giving economic model predictive control (EMPC). Chan and Chen investigated EMPC for an absorber-stripper system by including the cost of solvent and utilities in the objective function [34]. In addition to the solvent cost, Ma et al. considered the cost of carbon emissions in their EMPC [35]. Yu and Biegler applied a regularization approach to give EMPC with stability guarantees [36]. The control framework was demonstrated for a bubbling fluidized-bed solid-sorbent CO_2 capture process and considered operational costs related to cooling water and purge gas in the economic term of the optimization problem. A comprehensive economic objective function was used by Patron and Ricardez-Sandoval for an MEA-based absorber connected to a fuel-fired power plant [37]. Energy, chemical and utility costs as well as the cost of emitting CO_2, income from selling captured CO_2 and non-market related negative effects of carbon emissions were considered. A real-time optimization routine solved a steady-state economic optimization problem to provide regular updates of the setpoints for the NMPC.

1.4. Knowledge gaps and scope of paper

The literature review shows that both decentralized and model predictive control approaches for post-combustion CO_2 capture have been extensively studied. However, previous studies are mostly limited to solvent-based systems, and to our knowledge process control of an MBTSA process for post-combustion CO_2 capture has not been considered. In addition, the dynamic behavior of a complete MBTSA system under typical disturbances from a power plant has not been reported in the literature. These two knowledge gaps will be addressed in this work.

The research objective of this work is to investigate control structures for the MBTSA process for post-combustion CO_2 capture. The focus is on simple, decentralized control structures. They have shown to be viable for control of post-combustion CO_2 capture and are easy to implement since no additional models or optimization routines are required to determine the control action. Furthermore, it is useful to establish a baseline for control of the MBTSA process that more advanced control approaches can be compared to in the future. We consider an activated carbon-based MBTSA process designed to capture CO_2 from a coal-fired power plant. The closed-loop behavior of different control combinations is studied based on step changes and ramps of flue gas flow as well as controller setpoint changes. Controller performance is quantified by settling times and steady-state deviation from the control targets. The analysis is based on a dynamic model of the moving bed system developed in gPROMS.

The article is structured as follows. In Section 2 the overall method and design basis is explained, before the principle, modelling and design of the moving bed temperature swing adsorption system are described. In Section 3, the choice of control combinations, tuning of controllers and controller test cases are described. Results are presented and discussed in Section 4. Conclusions and recommendations for further work are given in Section 5.

2. Moving bed temperature swing adsorption

2.1. Method

This work considers the application of the MBTSA process for capturing CO_2 from a coal-fired power plant. The flue gas specifications at nominal conditions, as reported in Table 1, were taken as reference for the design. It has been assumed that the flue gas is cooled and dried before entering the CO_2 capture unit, which increases the energy use of the system. However, since the energy performance is not used as a performance indicator in this work, this effect has been neglected. In addition, the flue gas is taken as a binary mixture of CO_2 and N_2, where it has been assumed that O_2 and Ar exhibit similar behavior as N_2 [11]. This assumption reduces the computational time of the MBTSA simulations and is not expected to significantly affect the behavior of the CO_2 capture process.

After designing the MBTSA process model (described in Section 2.3) for the nominal operating point, the dynamic behavior of the system at off-design conditions was studied through a series of simulations. The current study only considers the effect of variations in flue gas flow on the CO_2 capture system, neglecting the integration with the steam/water cycle of the power plant. No power plant model has been developed, and load variations are assumed to be represented by changes in the flue gas feed flow to the MBTSA process. The composition, temperature and pressure of the flue gas is kept constant in all scenarios. Four different control configurations are investigated. An overview of the methodology is given in Fig. 1.

2.2. Process description

The moving bed temperature swing adsorption process makes use of a solid adsorbent with the ability of: (i) removing the CO_2 from the flue gas by selectively adsorbing the CO_2 onto its surface, (ii) releasing the adsorbed CO_2 when heated to a certain temperature. The first of the two properties is what allows the separation of the CO_2 from the rest of the flue gas components, while the second is responsible for allowing extraction of a high purity CO_2 stream and the regeneration of the adsorbent.

The process, shown schematically in Fig. 2, is continuous and operated in a cyclic manner by circulating the adsorbent through different sections. In the adsorption section the sorbent particles fall downwards counter-currently to the flue gas so that the CO_2 is retained by the adsorbent while the rest of the flue gas is released to the atmosphere. When leaving the adsorption section, the adsorbent is loaded with CO_2 and is sent to the desorption section for regeneration. The desorption section is essentially an indirect-contact heat exchanger where heat is

Table 1
Nominal flue gas specifications.

Quantity	Value	Unit
Temperature	25	°C
Pressure	1.05	bar
Flowrate	57.68	kg/s
Composition:		
CO_2	14.82	vol%
N_2	85.18	vol%

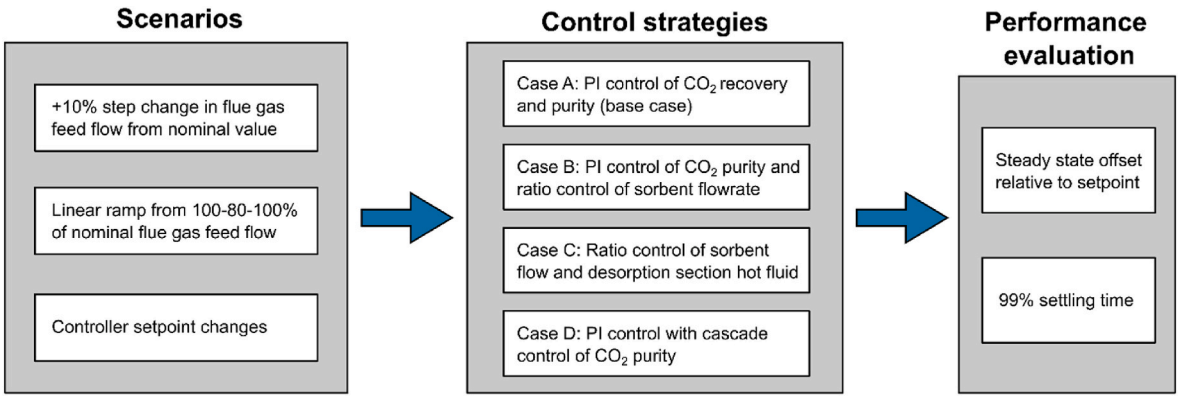

Fig. 1. Overview of methodology, including investigated scenarios, control strategies and controller performance evaluation.

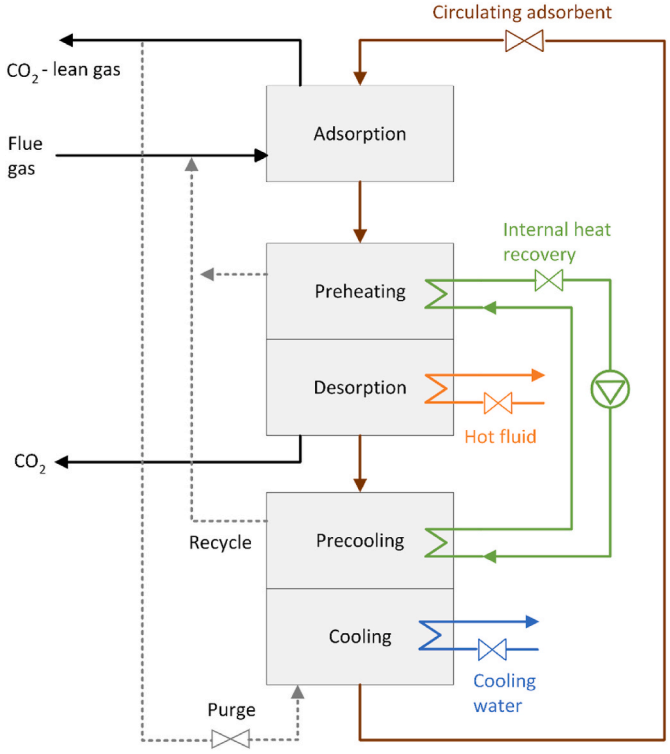

Fig. 2. Schematic diagram of the moving bed temperature swing adsorption (MBTSA) process. The manipulated variables to be used by the control system are indicated by valves.

provided to the adsorbent for promoting desorption of CO_2. As the temperature increases, the CO_2 is released by the adsorbent and can be withdrawn in a high purity stream. From the desorption section the unloaded adsorbent proceeds to the cooling section, which is again an indirect contact heat exchanger using cold water as media, where the temperature levels suitable for adsorption are restored. A fraction of the CO_2-lean gas leaving the adsorption section is recycled to the cooling section as a purge stream. After leaving the precooling section it is mixed with the flue gas feed to the adsorption section. The cooled adsorbent is finally collected and lifted back to the adsorption section with a conveyor belt system, so that the cycle is closed, and continuous system operation is maintained.

2.3. Mathematical model of MBTSA process

The MBTSA process was simulated with a previously developed model in gPROMS ModelBuilder version 6.0.4 [38]. Although it is dynamic, the model has previously only been used in steady-state design simulations. Therefore, the transient simulations from this work represent a novel application of the gPROMS model. A complete description of the model implementation and previous simulations can be found elsewhere [11], but for clarity the main characteristics of the model are described below. In addition, supplementary information is given in Appendix A.

The model makes use of the composite model capabilities of gPROMS to link the individual sections (adsorption, preheating, desorption, precooling and cooling section) via gas, solid and control signal ports. Each individual section is described by a set of partial differential equations (unsteady and one-dimensional) including mass, energy and momentum balances. In Table 2, a summary of the main model equations is given. Although the numerical value of certain design parameters (e.g., void fraction and section height) and operating conditions differ from section to section, the model equations and the underlying

Table 2
Summary of model equations used in gPROMS model of MBTSA process.

Mass balance in gas phase	$\varepsilon_c\frac{\partial C_i}{\partial t}+\frac{\partial (uC_i)}{\partial z}=\varepsilon_c\frac{\partial}{\partial z}\left(D_{z,i}C_T\frac{\partial Y_i}{\partial z}\right)-\frac{(1-\varepsilon_c-\xi)a' k_{f,i}}{\mathrm{Bi}_i/5+1}(C_i-C_{p,i})$	(1)
Mass balance in macropores	$\varepsilon_p\frac{\partial C_{p,i}}{\partial t}+\nu_s\frac{\partial C_{p,i}}{\partial z}=\varepsilon_p\frac{15D_{p,i}}{r_p{}^2}\frac{\mathrm{Bi}_i}{5+\mathrm{Bi}_i}(C_i-C_{p,i})-\rho_p\frac{15D_{c,i}}{r_c^2}(q_i^*-q_i)$	(2)
Mass balance in solid phase	$\frac{\partial q_i}{\partial t}+\nu_s\frac{\partial q_i}{\partial z}=\frac{15D_{c,i}}{r_c^2}(q_i^*-q_i)$	(3)
Momentum bal. (adsorption section)	$-\frac{\partial P}{\partial z}=(1-\varepsilon_c-\xi)a(\rho_p-\rho_g)$	(4)
Momentum bal. (other sections)	$-\frac{\partial P}{\partial z}=\frac{150\mu(1-\varepsilon_c)^2}{\varepsilon_c^3 d_p^2}u+\frac{1.75(1-\varepsilon_c)\rho_g}{\varepsilon_c^3 d_p}\lvert u\rvert u$	(5)
Energy balance in gas phase	$\varepsilon_c C_T\hat{c}_v\frac{\partial T}{\partial t}+uC_T\hat{c}_p\frac{\partial T}{\partial z}=\frac{\partial}{\partial z}\left(\lambda_g\frac{\partial T}{\partial z}\right)+\varepsilon_c RT\sum_i\frac{\partial C_i}{\partial t}-(1-\varepsilon_c-\xi)\,a'h_{gs}(T-T_s)-\alpha_{gt}h_{gw}(T-T_w)$	(6)
Energy balance in solid phase	$[(1-\varepsilon_c-\xi)\rho_p c_{p,s}+\xi\rho_{pk}c_{p,pk}]\left(\frac{\partial T_s}{\partial t}+\nu_s\frac{\partial T_s}{\partial z}\right)=(1-\varepsilon_c-\xi)\varepsilon_p RT_s\sum_i\left[\frac{\partial C_{p,i}}{\partial t}+\nu_s\frac{\partial C_{p,i}}{\partial z}\right]++\xi\frac{\partial}{\partial z}\left(\lambda_{pk}\frac{\partial T_s}{\partial z}\right)+(1-\varepsilon_c-\xi)a'h_{gs}(T-T_s)+(1-\varepsilon_c-\xi)\rho_p\sum_i\left(-\Delta H_i\left[\frac{\partial q_i}{\partial t}+\nu_s\frac{\partial q_i}{\partial z}\right]\right)$	(7)
Energy balance in the HX-wall	$\rho_w c_{p,w}\frac{\partial T_w}{\partial t}=\alpha_{w,ext}h_{gw}(T-T_w)-\alpha_{w,int}h_{fw}(T_w-T_f)$	(8)
Energy balance in the HX-fluid	$\rho_f c_{p,f}\frac{\partial T_f}{\partial t}=-u_f\rho_f c_{p,f}\frac{L_z}{L_x}\frac{\partial T_f}{\partial z}-\alpha_{w,int}h_{fw}(T_f-T_w)$	(9)
Adsorption equilibrium	$P_i=\frac{q_i^*}{K_i}\exp[\sum_{j=1}^N A_{ij}q_j^*+\sum_{j=1}^N\sum_{k=1}^N B_{ijk}q_j^*q_k^*]$	(10)
	$A_{ij}=\frac{A_i+A_j}{2};\ B_{ijk}=\frac{B_i+B_j+B_k}{3}$	(11)

assumptions are the same for each section. These include negligible gradients in the radial direction, constant cross-sectional area, constant sorbent velocity, uniform and constant void fraction, and ideal gas behaviour in the bulk phase. The mass transfer rate from the bulk gas to the adsorbent pores and from the pores to the adsorbed phase is modelled using linear driving force (LDF) approximations. With regards to the energy balances, the gas in the pores is assumed to be in thermal equilibrium with the adsorbent temperature, while the convective heat transfer between the bulk gas and the adsorbent is modelled with a heat transfer coefficient estimated with a common Nusselt correlation for flow around a sphere. In addition to the energy balance of the gas phase and the solid phase, two equations are included to describe the temperature of the heating/cooling fluid and the temperature of heat exchanger wall, respectively. This only applies to the sections that are operated as heat exchangers (preheating, desorption, precooling and cooling). The equation of the heat exchanger wall was derived by assuming that the thermal conduction resistance of the heat exchanger walls is negligible, while taking into account the effect of their thermal capacity. This approach is based on the consideration that the limiting thermal resistance of the system is found in the sorbent-gas side of the heat exchangers. The convection from the heating/cooling fluid to the wall is modelled with a constant heat transfer coefficient, representative of water flowing in tubes (5000 W/(m^2K)). Lastly, the convection from the wall to the gas is also modelled with a heat transfer coefficient. A value of 150 W/(m^2K) is assumed in this case.

2.4. Bead-shaped activated carbon adsorbent

The adsorbent material considered in the present study is a commercial bead-shaped activated carbon (BAC) supplied by Kurhea (Japan). It is well-suited for moving bed applications due to its particle size (0.7 mm average particle diameter) and highly spherical shape, which gives good flow properties. To provide necessary data for the MBTSA model, the adsorbent was characterized in terms of adsorption equilibrium by measuring pure component isotherms of CO_2 and N_2 at different temperatures between 10 and 150 °C. Prior the measurements the sample was pre-treated by applying vacuum for 10 h at a temperature of 150 °C. The collected data are shown in Fig. 2. As expected, the adsorbent presents higher affinity towards CO_2 compared to that of N_2, i.e., for a given temperature the adsorption capacity for CO_2 is higher than that of N_2 in the whole pressure range. However, at relevant temperature and pressure conditions, i.e., 25 °C, partial pressure of 15 kPa for CO_2, 85 kPa for N_2, the adsorption selectivity is relatively low due to the limited amount of CO_2 adsorbed (only about 0.5 mol/kg), and the significant amount of N_2 adsorbed (almost half of that of CO_2).

As shown in Fig. 3, the set of experimental data were fitted with a Virial isotherm model, of which parameters were then used as input to the gPROMS program.

The Virial model for pure component isotherms is given by:

$$P_i = \frac{q_i^*}{K_i}\exp\left(A_i q_i^* + B_i q_i^{*2}\right) \tag{12}$$

where P is the pressure, q is the amount of gas adsorbed, and K is the Henry constant. The latter was calculated with the Van't Hoff equation

$$K_i = K_i^{\infty}\left(\frac{-\Delta H_i}{RT_s}\right) \tag{13}$$

while the temperature dependence of the Virial coefficients A and B was expressed by

$$A_i = A_{0,i} + \frac{A_{1,i}}{T_s},\ B_i = B_{0,i} + \frac{B_{1,i}}{T_s}. \tag{14}$$

Fitting of the pure component adsorption data was carried out taking the data at all temperatures simultaneously. The resulting model parameters are listed in Table 3. The pure component parameters were used to simulate the multi-component separation by using the Virial model extension for multi-component gas mixtures.

2.5. Design and nominal performance

In Table 4, the design of the MBTSA system as well as the nominal operating conditions in the different sections are summarized. In the design, a cooling water inlet temperature of 10 °C and a heating fluid inlet temperature to the desorption section of 203 °C were assumed. The latter corresponds to a saturated steam pressure of around 16.5 bar. In Table 5, the overall process performance and additional operating conditions are given. Due to the somewhat low adsorption capacity of the adsorbent, a high amount of material (730 kg/s) was required to process the flue gas while capturing a large share of the incoming CO_2. In addition, the process was operated using a quite high regeneration temperature (above 180 °C), and a certain degree of vacuum (80 kPa) to extract the CO_2. The system delivers CO_2 with a purity of 95.4% with a CO_2 recovery rate of 81.7%. The CO_2 recovery is defined as:

$$\eta_{CO_2} = \frac{\dot{m}_{CO_2,out}}{\dot{m}_{CO_2,in}}. \tag{15}$$

Table 3
Virial isotherm model parameters for CO_2 and N_2 on the BAC adsorbent.

	K^{∞} x 10^6 mol/(kg kPa)	− ΔH kJ/mol	A_0 kg/mol	A_1 kg K/mol	B_0 (kg/mol)^2	B_1 kg^{2}K/mol^2
CO_2	1.8510	25.241	−0.294	243.088	0.035	−29.710
N_2	3.3827	17.185	−3.7245	1198.9	0	0

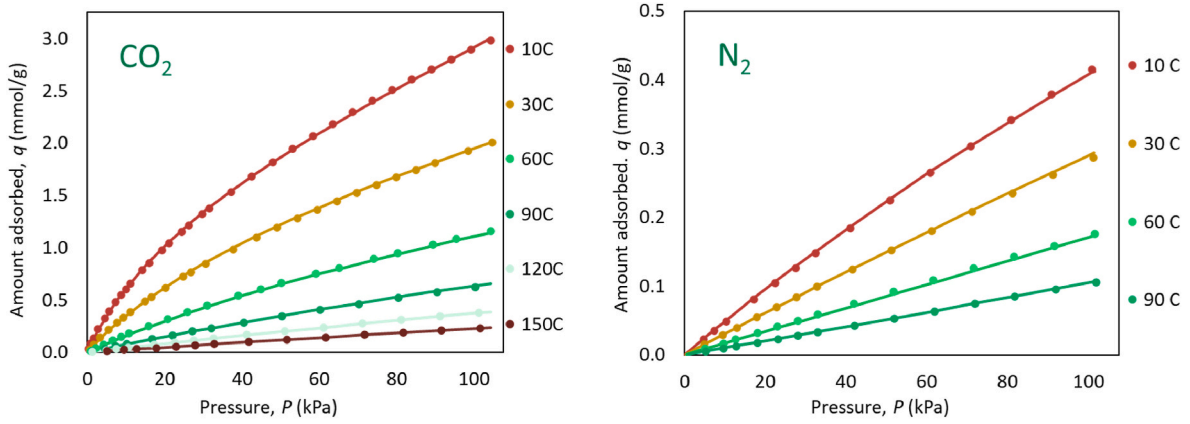

Fig. 3. Adsorption isotherms of CO_2 and N_2: measured data (dots) and Virial model fitting (continuous lines).

Table 4
Design parameters and nominal operating conditions in sections of the MBTSA.

		Adsorption	Preheating	Desorption	Precooling	Cooling
Section height	m	1.6	1.4	2.1	1.4	2.5
Section footprint (horizontal cross-sec.)	m^2	113	55	55	55	55
Sorbent residence time	s	33.6	30.3	45.5	30.3	54.2
Heating/cooling fluid inlet temperature	°C	–	149	203	64	10
Heating/cooling fluid outlet temperature	°C	–	64	135	149	75
Sorbent inlet temperature	°C	–	53	109	184	101
Sorbent outlet temperature	°C	–	109	184	101	24

Table 5
Overall process performance and main operating conditions.

Amount of circulating sorbent	730	kg/s
Sorbent regeneration temperature	184	°C
CO_2 extraction pressure	80	kPa
CO_2 purity	95.4	%
CO_2 recovery	81.7	%
CO_2 captured	10.2	kg/s
External heat duty (sorbent regeneration)	56.8	MW
Fraction of total heat recovered by inner loop	49.1	%
External cooling duty	53.8	MW_{th}
Specific heat duty	5.56	$MJ_{th}/kg\ CO_2$

Where $\dot{m}_{CO_2,in}$ is the mass flow of CO_2 entering the system via the flue gas feed and $\dot{m}_{CO_2,out}$ is the mass flow of CO_2 in the CO_2-rich stream leaving the desorption section.

3. Process control

In the MBTSA process considered in this work, there are five degrees of freedom that can be used as manipulated variables for process control. As shown in Fig. 1, these are the sorbent flow rate, flow rates of each of the three heat exchanger fluids (external heat, internal heat recovery loop and cooling water) and the flow rate of CO_2-lean gas used as purge in the cooling/precooling sections. Within the MBTSA model, the flow rates of the heat exchanger fluids are represented by their velocities.

3.1. Open-loop step responses

In order to choose CV-MV pairings and carry out controller tuning, it is necessary to investigate the open-loop behavior of the system. The control system was divided into a regulatory and a higher level. Simulations were performed by inactivating the higher-level controllers and introducing step changes in the main disturbance (flue gas feed flow) and manipulated variables. The regulatory layer remained active to ensure process stability. Due to the nonlinearity of the moving bed adsorption system, step changes of the same magnitude in opposite directions do not give opposite dynamic responses.

In Fig. 4, the response of CO_2 purity and recovery to a positive and negative 10% step in flue gas feed flow is shown. A reduction in the flue gas flow rate increases the sorbent to gas ratio in the adsorption section. As shown in the isotherms in Section 2.4, the activated carbon adsorbent is selective to CO_2 but also has considerable affinity for N_2. When the sorbent to gas ratio increases, an increase in the loading of N_2 and decrease in loading of CO_2 on the sorbent particles leaving the adsorption section is observed. The relative loading of CO_2 and N_2 on the sorbent influences the purity of the CO_2-rich gas leaving the desorption section. Therefore, a negative step change in the flue gas flow rate leads to a reduction in the CO_2 purity. The initial increase in the CO_2 recovery is caused by the sudden reduction of the denominator in Eq. (15). After approximately one cycle of the moving bed (3.2 min), the CO_2 recovery has stabilized at a 0.3% higher value than before the step change. This is due to the decrease in CO_2 loading on the particles leaving the adsorption section, which balances out the reduction in flue gas flow rate, thus ultimately leading to an almost unchanged CO_2 recovery.

When increasing the flue gas flow rate, the CO_2 recovery decreases due to a partial breakthrough of the moving bed. This means that at the bottom part of the adsorption section, the sorbent particles are saturated, and more CO_2 will pass through the column without being adsorbed. Since the relative loading of the adsorbed species is not significantly affected by the breakthrough, the CO_2 purity remains almost constant. The small change in purity can be explained by minor variations in adsorption section sorbent inlet temperature due to regulatory control and a slight decrease in inlet CO_2 concentration to the adsorption section caused by more flue gas being added relative to the recycled stream from the precooling section.

In Fig. 5, the open-loop responses of CO_2 purity to step changes in HX fluid velocity in the desorption section and CO_2 recovery to step changes in the sorbent flow rate are shown. Increasing or reducing the amount of heat supplied to the desorption section by 10% leads to a change in desorption section outlet sorbent temperature of ±3 °C. A higher desorption temperature leads to lower CO_2 loading on the sorbent entering the adsorption section, which will lead to a higher CO_2/N_2 ratio on the particles leaving this section. This will increase the CO_2 purity.

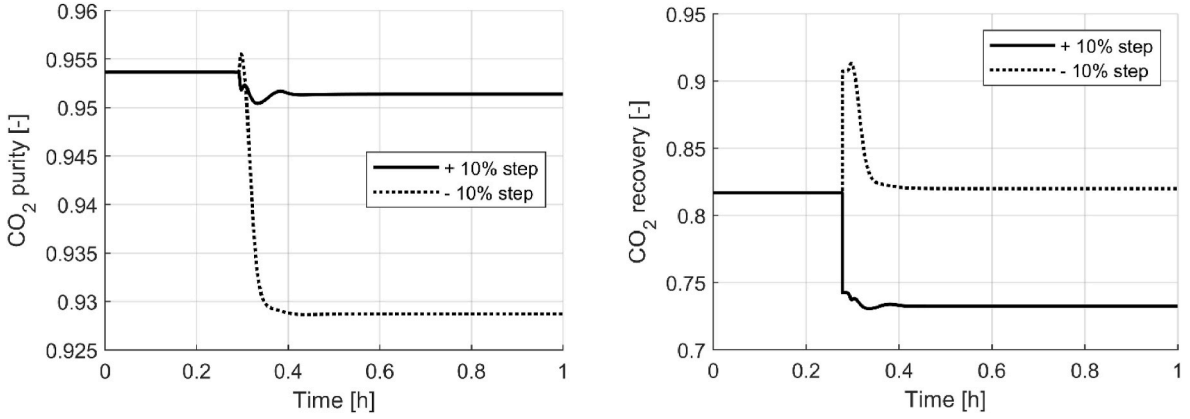

Fig. 4. Open-loop response of CO_2 purity (left) and recovery (right) to a positive and negative 10% step in flue gas flow.

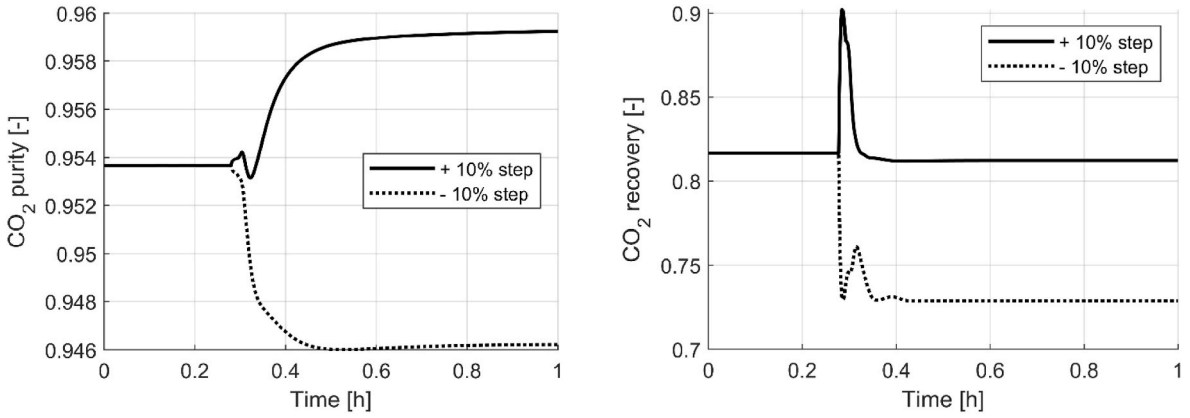

Fig. 5. Open-loop response of CO_2 purity (left) to a positive and negative 10% step in HX fluid velocity in the desorption section and open-loop response of CO_2 recovery (right) to a positive and negative 10% step in sorbent flow rate.

Reducing the HX fluid velocity has the opposite effect on the purity.

The effect of increasing the sorbent flow rate on CO_2 recovery is similar to the trend seen in Fig. 4 for a reduction in flue gas flow. After an initial increase, the system settles at a similar recovery rate as before the step change. In the adsorption section, an increase in sorbent inlet CO_2 loading and decrease in outlet CO_2 loading is observed, meaning that the working capacity of the adsorbent is reduced. The increase in inlet sorbent loading is caused by a reduction of the desorption temperature, since the heating of the desorption section remains unchanged. Reducing the sorbent flow rate leads to a partial breakthrough of the moving bed, leading to more CO_2 passing through the top of the adsorption section. This gives a reduction in CO_2 recovery of slightly below 9%.

3.2. Control combinations

The variable pairings were chosen based on heuristics and CV-MV step responses. Pairings for the regulatory layer, which in this case consists of three controllers, were chosen first. For the internal heat recovery loop, the velocity of working fluid was adjusted to maintain a constant ratio with the sorbent flow rate, to keep the fraction of heating/cooling delivered by the internal loop constant throughout operation. The temperature of the sorbent leaving the cooling section was controlled by adjusting the velocity of the cooling water flow. Finally, purge gas flow was adjusted to control the gas velocity at the top of the precooling section and prevent flow reversal. This phenomenon can occur as the adsorbent cools down and the CO_2 that is present in the pores is re-adsorbed, causing a local pressure reduction. Another phenomenon that should be avoided in the moving bed system is the fluidization of adsorbent particles. However, due to the large sorbent flow rates and particle size considered in this work, this is not expected to be an issue and fluidization has not been included in the regulatory control layer.

The regulatory layer leaves two degrees of freedom to be used for higher-level control. In this work, the CO_2 purity and recovery were chosen as control variables in this layer. The open-loop simulations in Section 3.1 show that varying the velocity of heating fluid to the desorption section influences the CO_2 purity and varying the sorbent flow rate affects the CO_2 recovery. These combinations were therefore chosen as CV-MV pairings in the higher-level control layer. As described in Section 1.2, this pairing follows the most common approach for control of post-combustion CO_2 capture processes.

Four control combinations are considered, namely Cases A, B, C and D. In Case A, PI-control is used for both higher-level control variables. The controllers were implemented using the PID controller block available in gPROMS ModelBuilder. The calculated value of the manipulated variable, u_{calc}, is given by the following equation:

$$u_{calc} = K_c(P + I)(u_{max} - u_{min}) + B \tag{16}$$

Where B is the controller bias, P is the contribution from the proportional term, I is the contribution from the integral term, u_{max} is the maximum allowable value of the manipulated variable and u_{min} is the minimum allowable value of the manipulated variable. The controller error, e, is defined as:

$$e = \frac{y_{SP} - y}{y_{max} - y_{min}} \tag{17}$$

Where y is the value of the controlled variable, and SP, max and min represent its setpoint, maximum and minimum allowable value. The proportional and integral terms are calculated based on the error:

$$P = e \tag{18}$$

$$\tau_I \frac{dI}{dt} = e \tag{19}$$

The MBTSA process is a cyclic process, meaning that there is significant delay between a control action is taken and its effect on the higher-level variables is seen. Such delays have a negative impact on the performance of feedback controllers. By adjusting the manipulated variables directly based on the disturbances, i.e. using feedforward control, this delay can be avoided. In this work, two feedforward control cases based on ratio control were investigated. The equation for such a controller is:

$$u_{calc} = \left(\frac{u}{d}\right)_{SP} d \tag{20}$$

Where d is the disturbance. In Case B, the sorbent flowrate is manipulated to maintain a given ratio between the sorbent flow rate and feed flue gas flow rate. The control of CO_2 purity is equal to Case A. Since a ratio controller has no feedback loop to gradually reduce the offset between the controlled variable and the setpoint, it is important to determine a correct ratio to avoid large steady-state offsets. It is likely that the optimal ratio will vary with operation. Steady-state simulations maintaining the desired purity and recovery at various loads were carried out to study the behavior of the ratio at off-design. The results are given in Fig. 6, and a linear trendline was used to adjust the ratio for the sorbent flow rate controller with the load.

In Case C, feedback control is given up entirely, and both higher-level controllers are ratio controllers. Since the sorbent flow rate is scaled adaptively based on the disturbance, a fixed ratio is used in the second controller, which adjusts the velocity of heating fluid to the desorption section based on the sorbent flow rate.

In Case D, we investigate a cascade controller for control of CO_2 purity. For CO_2 recovery, the same PI-controller as in Case A is used. A

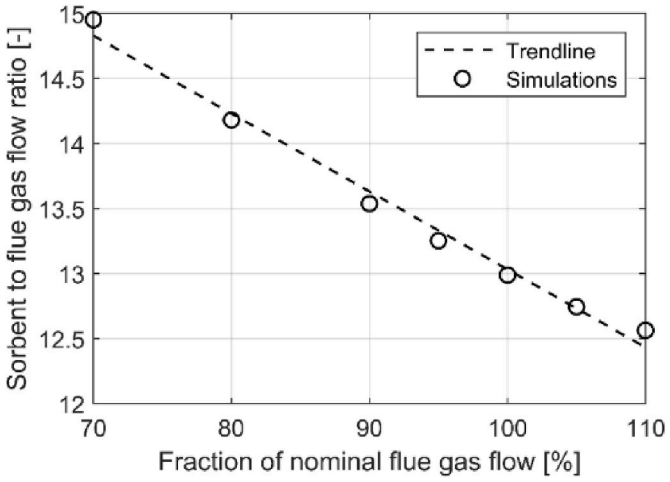

Fig. 6. Sorbent to flue gas feed flow ratio vs. fraction of nominal flue gas flow.

cascade control configuration makes use of an additional, fast measurement which is related to the controlled variable (in this case the sorbent temperature leaving the desorption section) with the aim of achieving faster control. An outer loop compares the CO_2 purity to the higher-level setpoint. Instead of adjusting the manipulated variable directly (as in Case A), the outer loop controller provides the setpoint to the inner loop, which adjusts the hot fluid velocity to the desorption section to control the outlet sorbent temperature. This configuration is shown in Fig. 7. The closed-loop time constant of the inner loop should be significantly smaller than the outer loop to avoid conflict between the two controllers. In this case the closed-loop time constant ratio of the two controllers is around 11.

The investigated control combinations with tuning parameters and setpoints are given in Table 6.

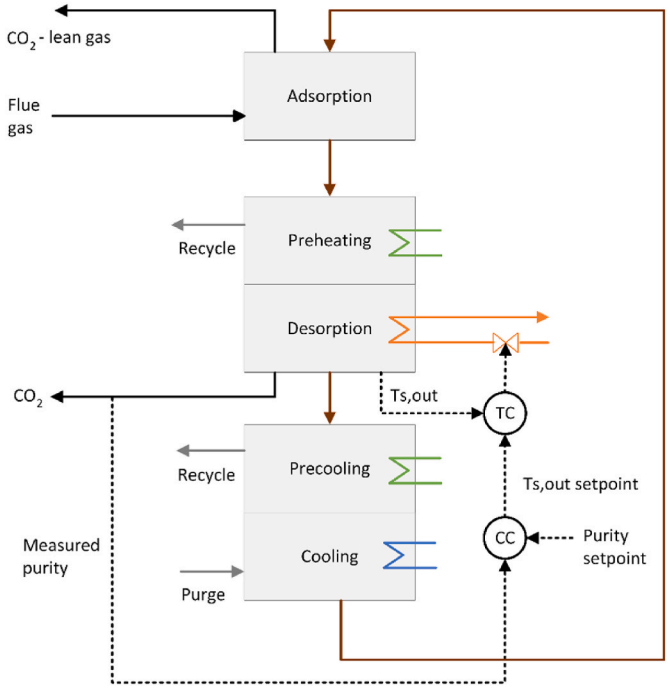

Fig. 7. CO_2 purity cascade control configuration studied in Case D. Dotted lines are signals, TC stands for temperature controller and CC stands for composition controller.

3.3. Tuning of PI-controllers

The tuning of the PI-controllers was based on the simplified internal model control (SIMC) rules developed by Skogestad [39]. For a PI-controller, a first-order transfer function between the MV and CV with effective delay is needed for the tuning:

$$g(s) = \frac{ke^{-\theta s}}{\tau s + 1} \tag{21}$$

Where k is the gain, θ is the effective delay and τ is the time constant of the transfer function $g(s)$ in the Laplace domain. The SIMC-rules give the controller gain K_c and the integral time constant τ_I using information from the transfer function and the adjustable closed-loop time constant τ_c:

$$K_c = \frac{1}{k}\frac{\tau}{\tau_c + \theta} \tag{22}$$

$$\tau_I = \min\lfloor \tau, 4(\tau_c + \theta)\rfloor. \tag{23}$$

Two different methods were used to obtain the transfer function. For simple responses that follow first-order behavior, the values were obtained graphically by inspection of the open-loop step response. The gain was taken as the difference between the initial and final value of the CV. The delay θ was taken as the time it took after the step in the MV before a continuous evolution of the CV in the same direction as the gain was observed. This means that any inverse responses are included in the effective delay. The time constant τ was taken as the time it took for the CV to reach 63% of its final value. When the open loop step response did not exhibit first-order behavior, the setpoint overshoot method using P-control [40] was applied. An example of the type of response used for tuning with this method is shown graphically in Fig. 8.

3.4. Controller testing and performance evaluation

Three types of simulations were performed to test the control combinations.

1) A positive 10% step change in flue gas feed flow from the nominal value
2) Linear ramps from 100 to 80 to 100% of nominal flue gas feed flow with slopes of 4% of nominal load per minute
3) Controller setpoint changes (for feedback controllers only)

The controller performance was quantified by the steady state offset relative to the setpoint and the 99% settling time, defined as the time it takes for the controlled variable to reach and stay within ±1% of the final steady-state value [23]. In all simulations, the time domain resolution was 5 s.

4. Results and discussion

4.1. Step on flue gas feed

In Fig. 9, the closed-loop responses of CO_2 purity and recovery as well as their corresponding manipulated variables to a +10% step on flue gas feed flow rate introduced at t = 0 are shown. An initial decrease in the CO_2 recovery rate is observed, since a larger fraction of the incoming CO_2 will leave at the top of the adsorption section before the sorbent flow rate is increased by the controller. The purity of the captured CO_2 is determined by the relative amounts of adsorbed CO_2 and N_2 on the adsorbent at the bottom of the desorption section, which is influenced by the adsorbent loadings out of the adsorption section and the heat provided to the preheating and desorption sections. The increased flue gas feed flow rate leads to a lower CO_2/N_2 ratio on the adsorbent, which gives the initial decrease in CO_2 purity.

Table 6
Summary of investigated cases for higher-level control and regulatory controllers with tuning parameters and setpoints.

Case	Description	CV	MV	τ_c (s)	K_c	τ_I (s)	Setpoint
A	PI control of both CO_2 purity and recovery (base case)	CO_2 purity	u_f desorption section	205	13.8	227	0.95
		CO_2 recovery	Sorbent flow	3.12	2.00	4.83	0.82
B	Ratio control of sorbent flowrate	CO_2 purity	u_f desorption section	205	13.8	227	0.95
		Sorbent/flue gas feed flow ratio	Sorbent flow	–	–	–	Adaptive
C	Ratio control of sorbent flowrate and hot fluid to desorption section	u_f/sorbent flow ratio desorption section	u_f desorption section	–	–	–	0.0023
		Sorbent/flue gas feed flow ratio	Sorbent flow	–	–	–	Adaptive
D	PI with cascade control of CO_2 purity	CO_2 purity (outer loop)	Setpoint for $T_{s,out}$ desorption section	205	13.8	227	0.95
		$T_{s,out}$ desorption section (inner loop)	u_f desorption section	18.5	0.34	74	From outer loop
		CO_2 recovery	Sorbent flow	3.12	2.00	4.83	0.82
	Regulatory control of cooling section sorbent outlet temperature	$T_{s,out}$ cooling section	u_f cooling section	15.4	−0.57	62	298 K
	Regulatory control of internal heat recovery loop	u_f/sorbent flow ratio in precooling and preheating sections	u_f internal heat recovery loop	–	–	–	0.0015
	Regulatory control of gas outlet velocity in pre-cooling section	u_{out} precooling section	Purge gas flowrate	2.2	13.6	2.2	0.078 m/s

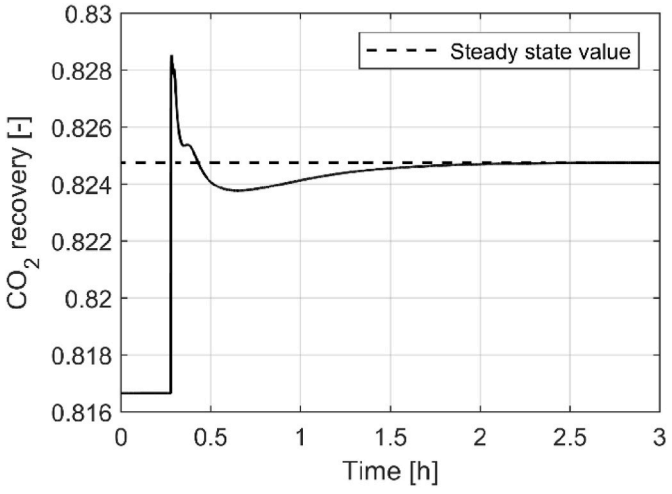

Fig. 8. Response of P-controlled CO_2 recovery with sorbent flow as MV to setpoint step from 0.82 to 0.83.

For purity control, Case C shows the quickest response, followed by Case A and B. The cascade controller in Case D reaches the desired setpoint but is not able to give a faster purity response than the standard PI configuration. The pure ratio control scheme in Case C is not able to precisely meet either the purity or recovery setpoint, but the final values are not far from the PI-controller setpoints. The sorbent flow ratio controller from Case B gives an absolute deviation of around 1% compared to the recovery setpoint. The overall best performance to the flue gas feed flow step change is achieved by Case A.

4.2. Flue gas flow ramps

The flue gas feed flow rate profile used in the simulations is showed in Fig. 10. The flow rate is first changed from 100 to 80% of nominal flow with a slope of 4% nominal flow per minute, before it is kept constant for several hours. After the controllers have stabilized, it is increased from 80 to 100% of nominal flow, keeping the same slope as for the ramp-down.

In Fig. 11, the response of both CVs and MVs in Case A-D from the ramp simulations are shown. The PI regulatory controllers are also included. Due to differences in the initialization of the model, the ratio control cases (Case B and C) start from slightly different values than Case A and D. This is, however, not expected to significantly influence the results. The reduction in flue gas flow rate leads to an increase of the CO_2 purity. As explained in section 4.1, the purity is governed by the ratio between adsorbed CO_2 and N_2 on the particles leaving the desorption section. Since the purity initially is higher than the setpoint, the heat supply to the desorption section is reduced. The adsorbed CO_2/N_2 ratio also depends on the temperature of the sorbent entering the adsorption section. Since the process is cyclic, this is equivalent to the temperature at the bottom outlet of the cooling section, which is controlled in the regulatory layer. For the negative flue gas flow ramp, this temperature is initially lower than the setpoint, and the flow of coolant in the cooling section is therefore reduced. The CO_2 recovery rate increases significantly when the flue gas feed flow is reduced, due to the sudden increase in solid to gas ratio in the adsorption section. The sorbent flow rate decreases by approximately 100 kg/s in order to bring the recovery rate to its setpoint. There is no delay between a change in the purge gas flow rate and the gas velocity in the pre-cooling section, which leads to only small variations in the value of this variable during the simulations. For all variables, the observed trends for the positive flue gas feed ramp are opposite of those described above for the negative ramp.

Regarding the controller performance, it is firstly seen that the regulatory control of both desorption section sorbent outlet temperature and precooling outlet gas velocity quickly stabilizes at the setpoint for both positive and negative ramps. The cascade controller in Case D generally uses a wider range of the manipulated variables than the other controllers but does not give improved performance. The response of sorbent temperature in Case A oscillates in the initial part of the response. Similar behavior is seen in the CO_2 purity profile, where the response in Case A oscillates initially. The use of ratio control (Case B) for sorbent flow rate shows no oscillations. As for the flue gas step, the purity controller in Case D exhibits the slowest response. The ratio controllers in Case C give a significantly larger steady-state offset for the ramp-down than the ramp-up case. In the latter case they are able to reach the setpoints for purity and recovery with similar accuracy as the feedback controllers. It is expected that the offsets of Case C could be significantly reduced by using an adaptive ratio also for the purity controller and by considering more accurate regression profiles than the linear trendline shown in Fig. 6. This would make it a more attractive option.

In the ramp simulations, Case A and B show the overall best performance. The oscillations seen in Case A could be caused by the PI controller tuning, which was carried out based on a positive step change from the nominal point. Since the behavior of the MBTSA process varies with load, these tunings might be too aggressive for the system at 80%,

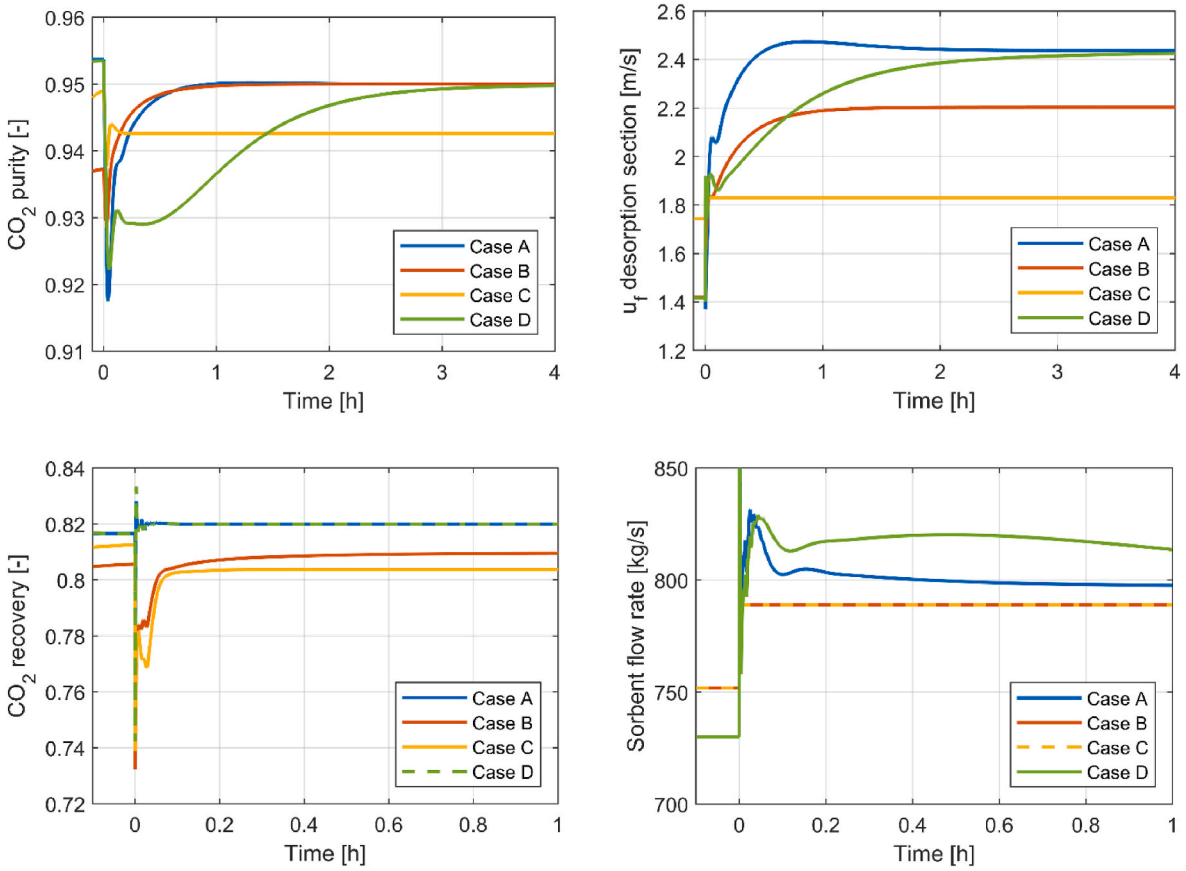

Fig. 9. Response of higher-level CVs (left) and MVs (right) to a 10% step on flue gas feed flow at t = 0.

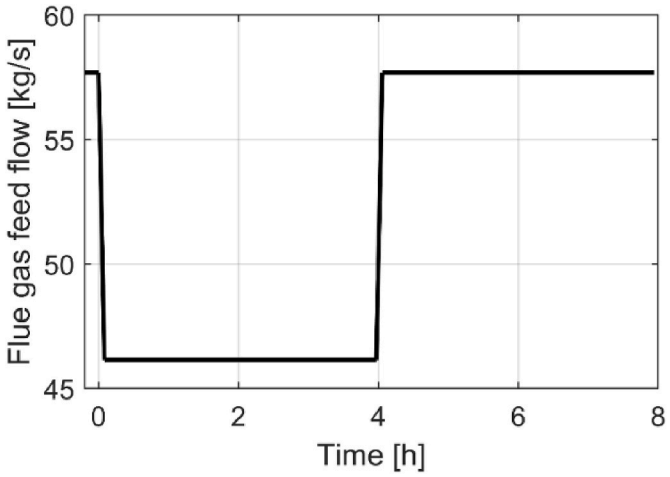

Fig. 10. Flue gas feed flow profile from the 100-80-100% ramp simulations.

giving an oscillatory response. For operation at loads below 80%, adaptive controller tuning might be necessary.

A simulation with one third of the original purity controller gain (K_c = 4.6) for Case A was carried out to demonstrate the effect of reduced gain on the oscillations. The results are shown in Fig. 12. It is seen that reducing the controller gain removes most of the oscillations but leads to larger over- and undershoot and slower regulation speed, especially for the ramp-up scenario. However, the purity control with reduced gain is still faster than Case D.

4.3. Step on controller setpoints

In Figs. 13 and 14, the higher-level controlled and manipulated variable responses to setpoint changes for purity (from 0.95 to 0.96) and recovery (from 0.82 to 0.83) introduced at t = 0 are shown. Only the PI-controllers are included in these graphs since the ratio controllers do not use the value of higher-level control variables as a setpoint. Case A shows the most efficient response to the purity setpoint change, followed by case B. The cascade controller in case D is not able to reach the new setpoint of 0.96 within the period of approximately 4 h used in the simulation, and in addition shows larger variations in sorbent flow rate than the standard PI-controller. Case A and D show similar responses to the recovery setpoint change, quickly adjusting to the new setpoint. These two cases have the same PI-controller for recovery control, and the similar response is therefore expected. The ratio used in the recovery controller of case B is not adaptively adjusted in the case of a purity setpoint change, since the flue gas feed flow remains constant. It is therefore not able to keep the recovery at the desired value of 0.82.

4.4. Summary of performance

In Table 7 and Table 8, the 99% settling time and steady state offset are given for the different cases for purity and recovery, respectively. For the flue gas flow step change, the settling time for CO_2 recovery is significantly shorter than for CO_2 purity in all cases except for the ratio control in Case C. Purity control is also significantly slower in the ramp simulations for Case A and D, which use PI control for the CO_2 recovery. The results show that ratio control can give around 10 times quicker purity control response and could therefore be a relevant option if response times are critical. The 99% settling time is in the order of minutes in all considered cases, apart from Case D. For this cascade

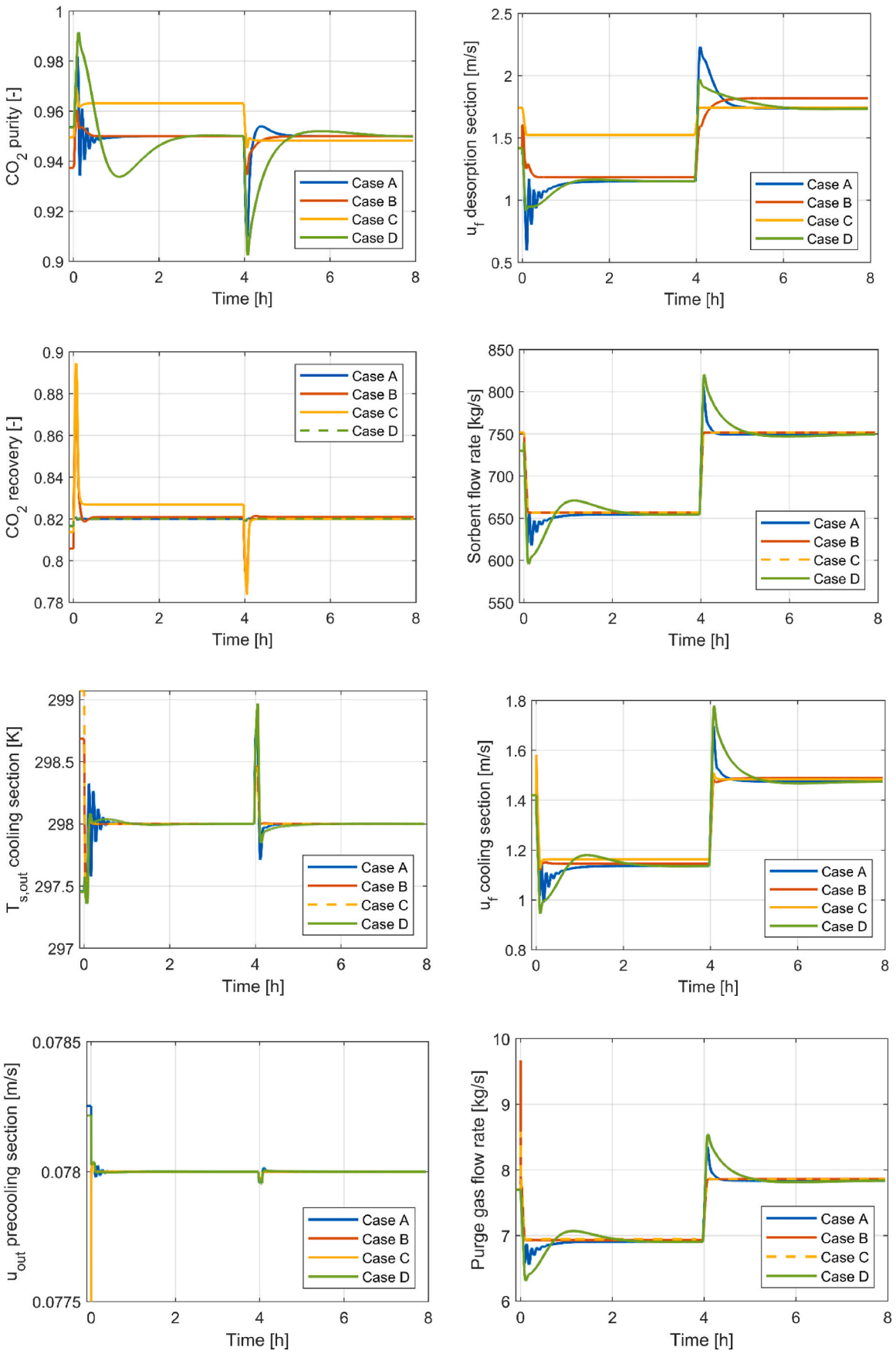

Fig. 11. Response of CVs (left) and MVs (right) to 100-80-100% flue gas feed flow ramps starting at t = 0.

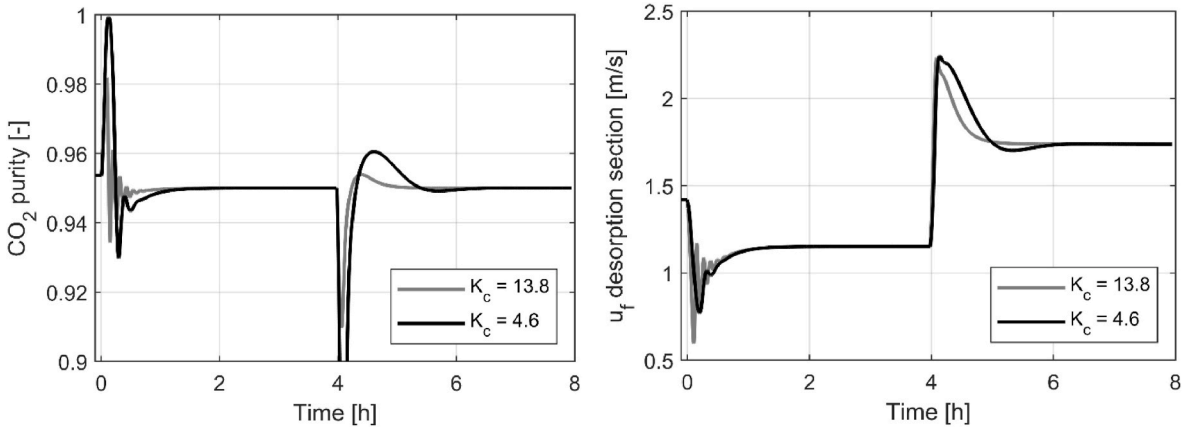

Fig. 12. Case A response of CO_2 purity and corresponding MV to 100-80-100% flue gas feed flow ramps starting at t = 0 with original (K_c = 13.8, grey line) and reduced (Kc = 4.6, black line) purity controller gain.

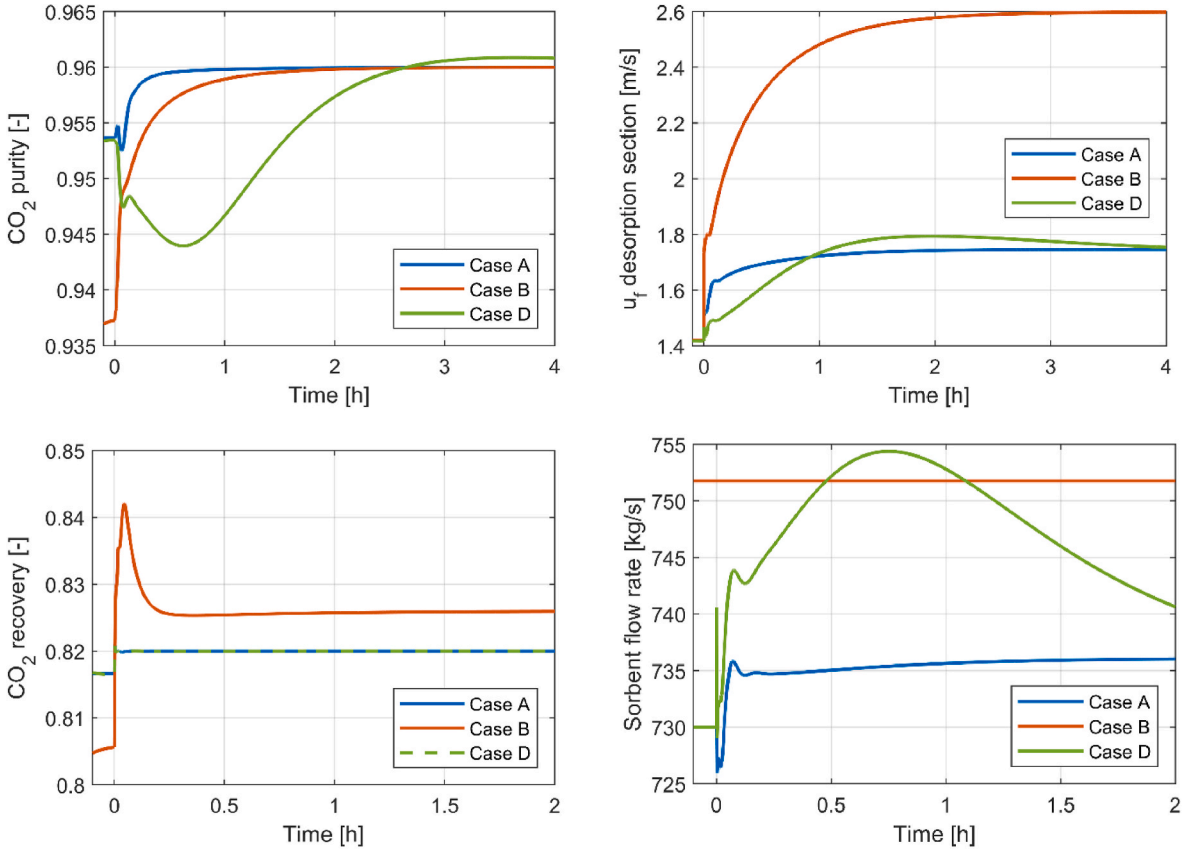

Fig. 13. Response of higher-level CVs (left) and MVs (right) to purity setpoint change from 0.95 to 0.96 at t = 0.

controller, the purity takes between 37 and 96 min to settle. In general, the controllers keep the controlled variables relatively close to the set-points. The largest steady state offset is 1.98% on CO_2 recovery from Case C in the flue gas step simulation.

CO_2 recovery settling times for solvent-based post-combustion CO_2 capture processes with similar control structures as in this work have been reported in many studies. Some values from the literature are mentioned below to put the results from this work into context. Montanes et al. reported 99.9% settling times between 45 and 400 min for a gas turbine ramp of 100–75-100% [23]. Gardardsdottir et al. observed 99% settling times around 100 min for 90-70-90% ramps on a coal-fired power plant [13]. Graphical estimation based on the results from Lin et al. shows a settling time of around 1 h for a 10% increase in flue gas flow rate [18]. In the work of Nittaya et al. [20], settling times from 7.5 to over 10 h for a 10% increase in flue gas flow rate were reported. The variations in settling times between studies are large, due to e.g. differences in system scales, modelling approach, underlying assumptions, ways of calculating settling time and scenarios used for controller testing. The settling times for CO_2 recovery found in this work are significantly shorter than values from the literature, indicating that the MBTSA process can be controlled efficiently. However, due to the reasons above, the values are not directly comparable, and a conclusion should not be made solely based on this work.

In this work, it has been assumed that all variables are available for

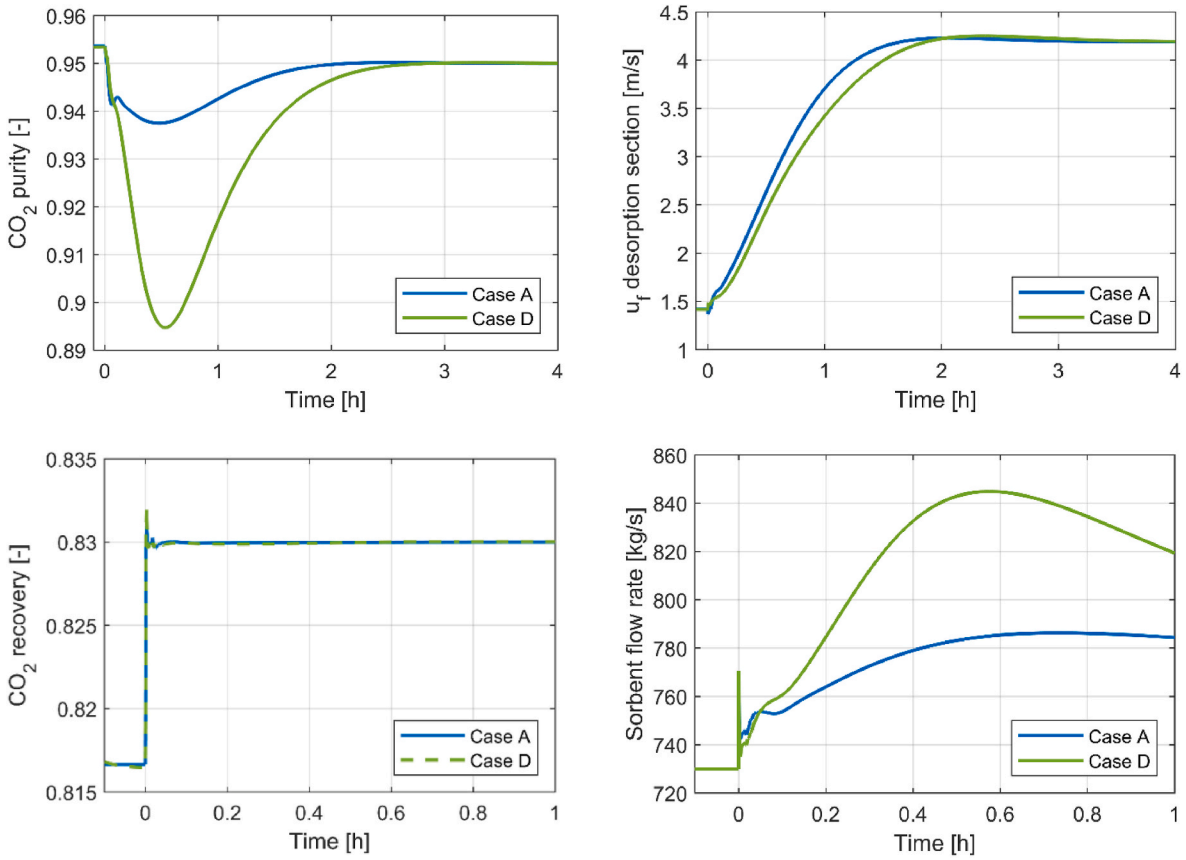

Fig. 14. Response of higher-level CVs (left) and MVs (right) to recovery setpoint from 0.82 to 0.83 at t = 0.

Table 7
CO_2 purity settling time and steady state offset for step change and ramps of flue gas feed flow. In cases with no reported settling time, the controlled variable did not move outside the ±1% range of the final value.

	+10% step on flue gas flow		Linear ramp 100-80%		Linear ramp 80–100%	
	99% settling time [min]	Steady-state offset (%)	99% settling time [min]	Steady-state offset (%)	99% settling time [min]	Steady-state offset (%)
Case A	11.3	0.00	12.8	0.00	10.3	0.00
Case B	6.00	0.00	5.42	0.00	7.50	0.00
Case C	–	0.78	1.33	1.38	1.58	0.18
Case D	75.3	0.02	95.5	0.01	37.1	0.01

Table 8
CO_2 recovery settling time and steady state offset for step change and ramps of flue gas feed flow. In cases with no reported settling time, the controlled variable did not move outside the ±1% range of the final value.

	+10% step on flue gas flow		Linear ramp 100-80%		Linear ramp 80–100%	
	99% settling time [min]	Steady-state offset (%)	99% settling time [min]	Steady-state offset (%)	99% settling time [min]	Steady-state offset (%)
Case A	0.17	0.00	–	0.00	–	0
Case B	3.42	1.26	8.00	0.12	7.50	0.12
Case C	2.67	1.98	7.42	0.85	7.58	0.01
Case D	0.25	0.00	–	0.00	–	0.00

measurement and that the measurements are without error and delay. In addition, no valve dynamics are considered when adjusting the manipulated variables. It is expected that this idealized approach will somewhat overestimate the performance of the controllers investigated. However, the model used in this work does consider important delays such as the transience of heating the walls of the different sections in the process, heating of gas and adsorbent and the cycling time of the adsorbent through the system. Another limitation of the proposed method is the fixed tuning parameters for the feedback controllers. In a practical application, the plant characteristics could change over time due to e.g. fouling, corrosion and particle degradation. In such cases, the controller tuning should be updated on-line.

5. Conclusions

In this work, four decentralized control strategies were investigated for an activated carbon-based MBTSA process designed to capture CO_2 from a coal-fired power plant. Through dynamic simulations with a composite model built in gPROMS, the closed-loop behavior of the control combinations was studied based on a step change and ramps of flue gas feed flow as well as controller setpoint changes.

The control system was divided into a regulatory and higher-level layer. The regulatory layer controls the internal heat recovery loop, sorbent outlet temperature of desorption section and outlet gas velocity of precooling section. It demonstrated fast response to both positive and negative ramps in flue gas feed flow and was able to keep the control

variables at their specified setpoint.

For the higher-level control layer, the standard PI configuration (Case A) generally showed the best response for both feed flow disturbances and setpoint changes. In this configuration, the CO_2 purity was controlled by the velocity of hot fluid to the desorption section and the sorbent flow rate was used to control the CO_2 recovery. The cascade controller (Case D) investigated for control of CO_2 purity was not able to give a faster purity response than the standard PI-configuration, and in addition showed wider input usage than the other controllers.

The two control configurations involving ratio control (Case B and C) in general gave larger steady-state offsets than the feedback controllers. However, in the case of ramp-up from 80 to 100% of nominal flue gas feed flow rate, these configurations yielded steady-state offsets in the same range as the PI-controllers. It is expected that the offset for other scenarios can be reduced by including an adaptive ratio also for purity control and by considering more accurate regression profiles. Due to their short stabilization time, ratio controllers might therefore be a viable control option for the MBTSA system.

In general, the settling time for CO_2 purity was longer than for CO_2 recovery. The 99% settling time for purity varied from 0 to 13 min in Cases A-C. Significantly slower responses were seen in Case D, with settling times for CO_2 purity ranging from 37 to 96 min approximately. For CO_2 recovery, the settling time varied from 0 to 8 min. The simulations show that using ratio controllers can give around 10 times quicker purity response compared to PI-control. All investigated control configurations were able to keep the controlled variables relatively close to the setpoints. The largest steady-state setpoint offset was 2.0%.

For ramp-down of flue gas feed flow from 100 to 80% of the nominal value, an oscillatory response was observed for Case A. This indicates that the controller tuning, which was based on +10% step responses from the nominal point, might not be suitable for lower loads. In this operation regime, adaptive PI-controller tunings might be necessary to avoid oscillations. This should be investigated in future work. In addition, simulations outside the 100-80% load range considered in this work will be necessary to test the effectiveness of the controllers in the case of wide operating changes. The current analysis does not consider measurement delays, assumes that all control variables are measurable and assumes that all manipulated variables can be adjusted instantaneously. This is expected to overestimate controller performance, and future investigations should therefore aim at including these additional delays and limitations in the modelling. In future work, it is also relevant to include additional performance indicators such as specific energy consumption in the evaluation of control configurations.

Credit author statement

V.T. Skjervold: Conceptualization, Formal analysis, Investigation, Methodology, Software, Visualization, Writing – original draft, G. Mondino: Conceptualization, Formal analysis, Funding acquisition, Investigation, Methodology, Software, Writing – review & editing, L. Riboldi: Methodology, Supervision, Writing – review & editing, L.O. Nord: Conceptualization, Funding acquisition, Methodology, Project administration, Supervision, Writing – review & editing.

Declaration of competing interest

The authors declare that they have no known competing financial interests or personal relationships that could have appeared to influence the work reported in this paper.

Data availability

Data will be made available on request.

Acknowledgements

We acknowledge financial support from the Polish-Norwegian Research Program for funding the InnCapPlant project (Grant NOR/POLNORCCS/0015/2019-00).

Nomenclature

ABBREVIATIONS

ARX	Autoregressive with exogeneous input
BAC	Bead-shaped activated carbon
CV	Controlled variable
EMPC	Economic model predictive control
LMPC	Linear model predictive control
MBTSA	Moving bed temperature-swing adsorption
MEA	Monoethanolamine
MPC	Model predictive control
MV	Manipulated variable
NARX	Non-linear autoregressive with exogeneous input
NGCC	Natural gas combined cycle
NMPC	Non-linear model predictive control
PI	Proportional-integral
SIMC	Simplified internal model control

LATIN SYMBOLS

a'	Particle specific area, $m^2\ m^{-3}$
A_i	First single-component Virial coefficient, kg mol^{-1}
A_{ij}	First multi-component Virial coefficient, kg mol^{-1}
B	Controller bias
B_i	Second single-component Virial coefficients of component i, $kg^2\ mol^{-2}$
B_{ij}	Second multi-component Virial coefficient, $kg^2\ mol^{-2}$
Bi_i	Biot number of component i
$c_{p,f}$	Specific heat of the heating/cooling fluid, J $kg^{-1}K^{-1}$
$c_{p,g}$	Specific heat of the gas mixture, J $kg^{-1}K^{-1}$

$c_{p,\mathrm{pk}}$	Specific heat of the packing material, J $kg^{-1}K^{-1}$
$c_{p,\mathrm{s}}$	Specific heat of the adsorbent, J $kg^{-1}K^{-1}$
$c_{p,\mathrm{w}}$	Specific heat of the heat exchanger tubes wall, J $kg^{-1}K^{-1}$
$\widehat{c}_p$	Molar heat of gas mixture at constant pressure, J mol^{-1} K^{-1}
$\widehat{c}_v$	Molar heat of gas mixture at constant volume, J mol^{-1} K^{-1}
C_i	concentration of component i in bulk gas phase, mol m^{-3}
$C_{\mathrm{p},i}$	concentration of component i in the macropores, mol m^{-3}
C_T	Total molar gas concentration in bulk phase, mol m^{-3}
d	Disturbance
$D_{\mathrm{c},i}$	Micropores/crystals diffusivity of component i, m^2 s^{-1}
$D_{\mathrm{p},i}$	Macropore diffusivity of component i, m^2 s^{-1}
$D_{\mathrm{z},i}$	Axial dispersion coefficient of component i, m^2 s^{-1}
e	Controller error, -
g	Transfer function
I	Controller integral term
k	Process gain
K_c	Controller gain
$k_{f,i}$	Film mass transfer coefficient of component i, m s^{-1}
K_i	Equilibrium constant of component i, mol kg^{-1} kPa^{-1}
K^∞	Equilibrium constant at infinite temperature, mol kg^{-1} kPa^{-1}
L_x	Tubes length along the flow direction, m
L_z	Tubes length along vertical axis, m
$\dot{m}$	Mass flow rate, kg s^{-1}
h_{gs}	Heat transfer coefficient between the gas and the solid, J $s^{-1}m^{-2}$ K^{-1}
h_{fw}	Heat transfer coefficient between the fluid and the tubes wall, J s^{-1} m^{-2} K^{-1}
h_{gw}	Heat transfer coefficient between the gas and the tubes wall, J $s^{-1}m^{-2}$ K^{-1}
P	Total pressure of the gas mixture, Pa
p	Controller proportional term
P_i	Partial pressure of component i, bar
q_i	Adsorbed phase concentration of component i, mol kg^{-1}
q_i^*	Adsorbed concentration of component i at equilibrium, mol kg^{-1}
R	Ideal gas constant, J $K^{-1}mol^{-1}$
r_c	Crystals/micropore radius, m
r_p	Particle radius, m
s	Laplace variable, s^{-1}
t	Time, s
T	Temperature of the gas phase, K
T_f	Temperature of the heating/cooling fluid, K
T_s	Temperature of the solid phase, K
T_w	Temperature of the heat exchanger tubes wall, K
u	Superficial gas velocity, m s^{-1}
u	Manipulated variable
v_s	Velocity of the solid phase, m s^{-1}
y	Controlled variable
Y_i	Molar fraction of component i
z	Axial coordinate along the section height, m

GREEK SYMBOLS

α_{gt}	Ratio of external surface area of tubes to gas-solid volume, m^2m^{-3}
$\alpha_{\mathrm{w,ext}}$	Ratio of external surface area of tubes to gas-solid volume, m^2m^{-3}
$\alpha_{\mathrm{w,int}}$	Ratio of internal surface area of tubes to gas-solid volume, m^2m^{-3}
ΔH_i	Heat of adsorption of component i, J mol^{-1}
ε_c	Column void fraction, -
ε_p	Particle porosity, -
η_{CO_2}	CO_2 capture (recovery) rate , -
θ	Effective delay, s
λ_g	Axial heat dispersion coefficient of the gas mixture, W m^{-1} K^{-1}
λ_{pk}	Axial heat dispersion coefficient of the structured packing, W m^{-1} K^{-1}
ξ	Volumetric fraction of the structured packing, -
ρ_f	Density of heating/cooling fluid, kg m^{-3}
ρ_g	Density of the gas mixture, kg m^{-3}
ρ_p	Density of adsorbent particles, kg m^{-3}
ρ_{pk}	Density of the structured packing, kg m^{-3}
ρ_w	Density of heat exchanger tubes wall, kg m^{-3}

τ_c Closed-loop time constant, s
τ_I Controller integral time, s

Appendix A. Supplementary information on gPROMS model

In Table A1 and Table A2, supplementary information on the gPROMS model is given.

Table A1
Values of fixed parameters and solver-related information from gPROMS model.

Parameter	Value	Unit	Parameter	Value	Unit
ρ_f	1000	kgm^{-3}	$c_{p,f}$	4200	J kg^{-1} K^{-1}
ρ_p	904	kgm^{-3}	$c_{p,pk}$	500	J kg^{-1} K^{-1}
ρ_{pk}	1000	kgm^{-3}	$c_{p,s}$	880	J kg^{-1} K^{-1}
ρ_w	4420	kgm^{-3}	$c_{p,w}$	526	J kg^{-1} K^{-1}
ε_c (ads sec.)	0.8	–	h_{fw}	5000	W m^{-2} K^{-1}
ε_c (other sec.)	0.5	–	h_{gw}	150	W m^{-2} K^{-1}
ε_p	0.5	–	L_x	52.8	m
ξ	0.05	–	L_z	1	m
λ_{pk}	0.001	W m^{-1} K^{-1}			
Number of discretization points					
Precooling	200	–			
Cooling	100	–			
Preheating	100	–			
Desorption	100	–			
Adsorption	200	–			
Discretization method		Central finite difference			
Differential-algebraic solver		SRADAU			
Linear algebra solver		MA28			
Absolute tolerance		1E-8			
Relative tolerance		1E-8			

Table A2
Correlations used in gPROMS model, from Ref. [11].

Binary diffusivity	$D_{ij} = \frac{0.01883T^{3/2}}{P\sigma_{ij}^2\Omega_{D_{ij}}}\sqrt{\frac{1}{M_{w,i}}+\frac{1}{M_{w,j}}}$
Molecular diffusivity	$D_m = \frac{1-y_i}{\sum_{j\neq i}^{n}\frac{y_j}{D_{ij}}}$
Knudsen diffusivity	$D_k = 97r_p\sqrt{\frac{T}{M_w}}$
Macropore diffusivity	$\frac{1}{D_p} = \tau_p\left(\frac{1}{D_k}+\frac{1}{D_m}\right)$
Axial dispersion coefficient	$D_z = \frac{D_m}{\varepsilon_c}(20 + 0.5\,\mathrm{Sc}\,\mathrm{Re})$
Adsorption rate in micropores	$\frac{D_c}{r_c^2} = \frac{D_c^0}{r_c^2}\exp\left(-\frac{E_a}{RT}\right)$
Axial thermal conductivity of gas	$\lambda_g = k_g(7 + 0.5\,\mathrm{Pr}\,\mathrm{Re})$
Sherwood number correlation	$\mathrm{Sh} = 2.0 + 1.1\mathrm{Re}^{0.6}\mathrm{Sc}^{1/3}$
Nusselt number correlation	$\mathrm{Nu} = 2.0 + 1.1\mathrm{Re}^{0.6}\mathrm{Pr}^{1/3}$

References

[1] IEA. World energy outlook 2020. 2020 [Online]. Available: https://www.iea.org/reports/world-energy-outlook-2020. Paris.
[2] Richter M, Möllenbruck F, Starinsk A, Oeljeklaus G, Görner K. Flexibilization of coal-fired power plants by dynamic simulation. Proceedings of the 11th International Modelica Conference, Versailles, France, Sept. 21-23 2015;118:715–23. https://doi.org/10.3384/ecp15118715. 2015.
[3] Gonzalez-Salazar MA, Kirsten T, Prchlik L. Review of the operational flexibility and emissions of gas- and coal-fired power plants in a future with growing renewables. Renew Sustain Energy Rev 2018;82(July 2017):1497–513. https://doi.org/10.1016/j.rser.2017.05.278.
[4] United Nations Department of Economic and Social Affairs. Sustain Dev Goal 2022;7. accessed Feb. 16, 2022), https://sdgs.un.org/goals/goal7.
[5] IPCC, "Global Warming of 1.5°C. An IPCC Special Report on the impacts of global warming of 1.5°C above pre-industrial levels and related global greenhouse gas emission pathways. In: The context of strengthening the global response to the threat of climate change; 2018.
[6] Feron PHM, Cousins A, Jiang K, Zhai R, Garcia M. An update of the benchmark post-combustion CO_2-capture technology. Fuel 2020;273(February):117776. https://doi.org/10.1016/j.fuel.2020.117776.
[7] Samanta A, Zhao A, Shimizu GKH, Sarkar P, Gupta R. Post-combustion CO_2 capture using solid sorbents: a review. Ind Eng Chem Res 2012;51(4):1438–63. https://doi.org/10.1021/ie200686q.
[8] Kim H, Miller D, Modekurti S, Omell B, Bhattacharyya D, Zitney S. Mathematical modeling of a moving bed reactor for post-combustion CO_2 capture. AIChE J 2016;62(11):3899–914.
[9] Morales-Ospino R, et al. Parametric analysis of a moving bed temperature swing adsorption (MBTSA) process for postcombustion CO_2 capture. Ind Eng Chem Res 2021. https://doi.org/10.1021/acs.iecr.0c05067.
[10] Mondino G, Grande CA, Blom R. Effect of gas recycling on the performance of a moving bed temperature-swing (MBTSA) process for CO_2 capture in a coal fired power plant context. Energies 2017;10(6). https://doi.org/10.3390/en10060745.
[11] Mondino G, Grande CA, Blom R, Nord LO. Moving bed temperature swing adsorption for CO_2 capture from a natural gas combined cycle power plant. Int J Greenh Gas Control 2019;85(October 2018):58–70. https://doi.org/10.1016/j.ijggc.2019.03.021.

[12] Wu X, Wang M, Liao P, Shen J, Li Y. Solvent-based post-combustion CO_2 capture for power plants: a critical review and perspective on dynamic modelling, system identification, process control and flexible operation. Appl Energy 2020;257 (October 2019):113941. https://doi.org/10.1016/j.apenergy.2019.113941.
[13] Gardarsdóttir S, Montañés RM, Normann F, Nord LO, Johnsson F. Effects of CO_2-absorption control strategies on the dynamic performance of a supercritical pulverized-coal-fired power plant. Ind Eng Chem Res 2017;56(15):4415–30. https://doi.org/10.1021/acs.iecr.6b04928.
[14] Cormos AM, Vasile M, Cristea MV. Flexible operation of CO_2 capture processes integrated with power plant using advanced control techniques. Comput Aided Chem Eng 2015;37(June):1547–52. https://doi.org/10.1016/B978-0-444-63577-8.50103-0.
[15] Panahi M, Skogestad S. Economically efficient operation of CO_2 capturing process. Part II. Design of control layer. Chem Eng Process: Process Intensif 2012;52: 112–24. https://doi.org/10.1016/j.cep.2011.11.004.
[16] Gaspar J, Ricardez-Sandoval L, Jørgensen JB, Fosbøl PL. Controllability and flexibility analysis of CO_2 post-combustion capture using piperazine and MEA. Int J Greenh Gas Control 2016;51:276–89. https://doi.org/10.1016/j.ijggc.2016.06.003.
[17] Lawal A, Wang M, Stephenson P, Koumpouras G, Yeung H. Dynamic modelling and analysis of post-combustion CO_2 chemical absorption process for coal-fired power plants. Fuel 2010;89(10):2791–801. https://doi.org/10.1016/j.fuel.2010.05.030.
[18] Lin YJ, Pan TH, Wong DSH, Jang SS. Plantwide control of CO_2 capture by absorption and stripping using monoethanolamine solution. Ind Eng Chem Res 2011;50(3):1388. 1345.
[19] Mechleri ED, Biliyok C, Thornhill NF. Dynamic simulation and control of post-combustion CO_2 capture with MEA in a gas fired power plant. In: Proceedings of the 24th European symposium on computer aided process engineering - ESCAPE 24; 2014. Budapest, Hungary, June 15-18.
[20] Nittaya T, Douglas PL, Croiset E, Ricardez-Sandoval LA. Dynamic modelling and control of MEA absorption processes for CO_2 capture from power plants. Fuel 2014; 116:672–91. https://doi.org/10.1016/j.fuel.2013.08.031.
[21] Cristea VM, Burca MI, Ilea FM, Cormos AM. Efficient decentralized control of the post combustion CO_2 capture plant for flexible operation against influent flue gas disturbances. Energy 2020;205:117960. https://doi.org/10.1016/j.energy.2020.117960.
[22] Mechleri E, Lawal A, Ramos A, Davison J, Mac Dowell N. Process control strategies for flexible operation of post-combustion CO_2 capture plants. Int J Greenh Gas Control 2017;57:14–25. https://doi.org/10.1016/j.ijggc.2016.12.017.
[23] Montañés RM, GarÐarsdóttir S, Normann F, Johnsson F, Nord LO. Demonstrating load-change transient performance of a commercial-scale natural gas combined cycle power plant with post-combustion CO_2 capture. Int J Greenh Gas Control 2017;63(April):158–74. https://doi.org/10.1016/j.ijggc.2017.05.011.
[24] Lawal A, Wang M, Stephenson P, Obi O. Demonstrating full-scale post-combustion CO_2 capture for coal-fired power plants through dynamic modelling and simulation. Fuel 2012;101:115–28. https://doi.org/10.1016/j.fuel.2010.10.056.
[25] Wu X, Shen J, Wang M, Lee KY. Intelligent predictive control of large-scale solvent-based CO_2 capture plant using artificial neural network and particle swarm optimization. Energy 2020;196:117070. https://doi.org/10.1016/j.energy.2020.117070.
[26] Rúa J, Hillestad M, Nord LO. Model predictive control for combined cycles integrated with CO_2 capture plants. Comput Chem Eng 2021;146. https://doi.org/10.1016/j.compchemeng.2020.107217.
[27] Jung H, Im D, Heo S, Kim B, Lee JH. Dynamic analysis and linear model predictive control for operational flexibility of post-combustion CO_2 capture processes. Comput Chem Eng 2020;140. https://doi.org/10.1016/j.compchemeng.2020.106968.
[28] Li Q, Zhang W, Qin Y, An A. Model predictive control for the process of mea absorption of CO_2 based on the data identification model. Processes 2021;9(1): 1–16. https://doi.org/10.3390/pr9010183.
[29] Jung H, Heo S, Lee JH. Model predictive control for amine-based CO_2 capture process with advanced flash stripper. Control Eng Pract 2021;114(June):104885. https://doi.org/10.1016/j.conengprac.2021.104885.
[30] Sultan T, Zabiri H, Shahbaz M, Maulud AS. Performance evaluation of the fast model predictive control scheme on a CO_2 capture plant through absorption/stripping system. Process Saf Environ Protect 2022;157:218–36. https://doi.org/10.1016/j.psep.2021.11.018.
[31] Akinola TE, Oko E, Wu X, Ma K, Wang M. Nonlinear model predictive control (NMPC) of the solvent-based post-combustion CO_2 capture process. Energy 2020; 213:118840. https://doi.org/10.1016/j.energy.2020.118840.
[32] Patron GD, Ricardez-Sandoval L. A robust nonlinear model predictive controller for a post-combustion CO_2 capture absorber unit. Fuel 2020;265(December 2019): 116932. https://doi.org/10.1016/j.fuel.2019.116932.
[33] Mejdell T, Kvamsdal HM, Hauger SO, Gjertsen F, Tobiesen FA, Hillestad M. Demonstration of non-linear model predictive control for optimal flexible operation of a CO_2 capture plant. Int J Greenh Gas Control 2022;117(September 2021):103645. https://doi.org/10.1016/j.ijggc.2022.103645.
[34] Chan LLT, Chen J. Improving the energy cost of an absorber-stripper CO_2 capture process through economic model predictive control. Int J Greenh Gas Control 2018;76(July):158–66. https://doi.org/10.1016/j.ijggc.2018.05.018.
[35] Ma C, Zhang W, Zheng Y, An A. Economic model predictive control for post-combustion CO_2 capture system based on MEA. Energies 2021;14(23):1–15. https://doi.org/10.3390/en14238160.
[36] Yu M, Biegler LT. Economic NMPC strategies for solid sorbent-based CO_2 capture. IFAC-PapersOnLine 2018;51(18):103–8. https://doi.org/10.1016/j.ifacol.2018.09.283.
[37] Patrón GD, Ricardez-Sandoval L. An integrated real-time optimization, control, and estimation scheme for post-combustion CO_2 capture. Appl Energy September 2021; 308:2022. https://doi.org/10.1016/j.apenergy.2021.118302.
[38] PSE. gPROMS ModelBuilder 2022. https://www.psenterprise.com/products/gproms/modelbuilder. [Accessed 19 February 2022]. accessed.
[39] Skogestad S. Simple analytic rules for model reduction and PID controller tuning. J Process Control 2003;13:291–309. https://doi.org/10.4173/mic.2004.2.2.
[40] Shamsuzzoha M, Skogestad S. The setpoint overshoot method: a simple and fast closed-loop approach for PID tuning. J Process Control 2010;20(10):1220–34. https://doi.org/10.1016/j.jprocont.2010.08.003.